ISSN 1063-7710, Acoustical Physics, 2024, Vol. 70, No. 1, pp. 82–89. © The Author(s), 2024. This article is an open access publication.

PHYSICAL ACOUSTICS

Phase Correction of the Channels of a Fully Populated Randomized Multielement Therapeutic Array Using the Acoustic Holography Method

S. A. Tsysar[a], *, P. B. Rosnitskiy[a], S. A. Asfandiyarov[a], S. A. Petrosyan[a], V. A. Khokhlova[a], and O. A. Sapozhnikov[a]

[a] *Faculty of Physics, Moscow State University, Moscow, 119991 Russia*

**e-mail: sergey@acs366.phys.msu.ru*

Received November 26, 2023; revised December 18, 2023; accepted December 19, 2023

Abstract—The acoustic holography method was used to characterize a therapeutic focused fully populated 256-element ultrasonic transducer array. Elements of the array with the shape of equal area polygons are densely arranged in an irregular pattern on a spherically concave surface with a radius of curvature of 150 mm and a diameter of 200 mm. The array has a central frequency of 1.2 MHz and is designed to operate in water. The performance of individual array elements was studied based on the holographically reconstructed normal velocity distribution over the array surface. It was shown that with the same electrical signals applied to the elements, their acoustic responses had a phase deviation relative to the nominal values, which can be caused either by the asphericity of the array surface, or by the introduction of additional phase delays by the electrical matching network. To compensate for the detected parasitic phase shifts of the elements and restore the effective sphericity of the radiating surface, the Verasonics V-1 control system was used. The hologram measured after making the correction, as well as the shape of the focal region and acoustic pressure magnitude at the focus, separately measured by a hydrophone, showed that the proposed method reconstructed the nominal operating parameters of the array with high accuracy.

Keywords: acoustic holography, mosaic gratings, fully populated arrays, transducer characterization, phase correction

DOI: 10.1134/S1063771023601280

INTRODUCTION

With the development of control systems for low-intensity diagnostic and high-intensity focused multi-element ultrasound transducers, the range of applications in both medicine and industry is expanding. Various therapeutic applications of ultrasound that have been actively developed in recent years can be highlighted. One of them is thermal ablation aimed for a rapid localized tissue heating which causes subsequent thermal denaturation of the targeted tissue [1, 2]. Another one is ultrasonic histotripsy aimed for mechanical (non-thermal) localized destruction of biological tissues [3–6]. Among diagnostic applications, which utilize relatively intense focused ultrasound, it is important to note the elastography method based on measuring the propagation speed of shear waves (shear waves elastography, SWE) generated in the focal region of the transducer [7–9]. All these applications require high precision ultrasonic field exposure to the object or media in order to minimize the risks of tissue damage outside the area of interest. This is possible if complete information is known about the parameters of each radiating element and the structure of the field created by the multi-element system. However, in many cases, the vibration structure of piezoelectric elements is usually unknown and often differs from the widely used piston source approximation [10]. The real structure of the field along the transducer surface can be determined using the acoustic holography method [10, 11]. This method allows for solving the inverse problem for a monochromatic field by measuring the amplitude and phase of the acoustic pressure over some surface (i.e., hologram) in front of the ultrasound source. Subsequently, the boundary condition at the surface of the transducer can be reconstructed by backpropagating the measured field and then used for forward propagation simulations to determine the 3D structure of the radiated field without relying on rough approximations. The holography approach can be extended to the transient case for the pulsed field characterization [12].

For multi-channel receiving-emitting systems it is important to know not only the structure of the surface vibrations of the elements, but also the characteristics of all electrical components for each channel that affect the electrical signal and, ultimately, the resulting

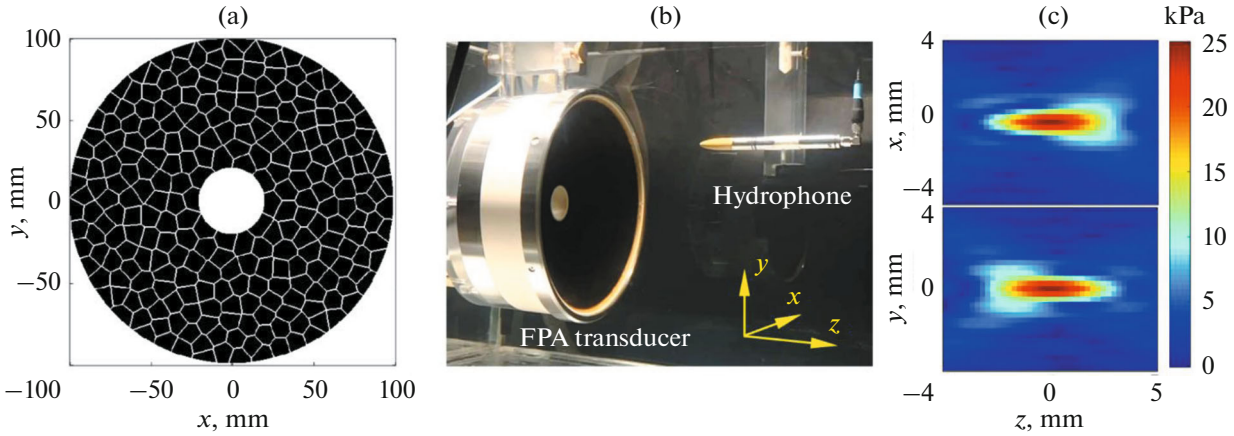

Fig. 1. Fully populated 256-element ultrasonic transducer array (FPA). (a) Schematics of element arrangement along the transducer surface. (b) Photograph of the FPA in a water tank during the measurements with the HGL-0200 hydrophone. (c) Measured acoustic pressure distributions in the focal region for horizontal *XZ* (top) and vertical *YZ* (bottom) sections with 0.25 mm step at Verasonics Data Acquisition system (VDAS) input levels of 3.6 V for in-phase excitation mode.

acoustic field. It is also important to note that the nature of surface vibrations, even within one selected element, will, in general, be different for different modes of operating the transducer. For example, for a two-dimensional diagnostic probe [12] operating in in-phase mode, the oscillation of the surface of one element can be almost uniform, while in operating modes with a noticeable phase shift between the elements, the amplitude of the surface vibration of each element will noticeably decrease towards the edges. The change in the structure of the vibration pattern when using the electronic control of the beamforming depends on the design of the multi-element transducer, the type of piezoelectric material, the dimensions of individual elements, and a number of other factors [11–14]. Therefore, to fully characterize multi-element systems it is necessary to carry out measurements at all possible amplitude values and phase shifts between elements to take into account all mechanisms of the elements interaction. In reality, it is advisable to carry out measurements for the in-phase excitation mode of elements and for several positions of the electronic focus (or beam, for unfocused transducers) steering [15, 16]. This approach allows to examine the integrity of the source, identify deviations in the operation of channels, and detect the presence of defects that affect the radiated acoustic field. The use of multi-channel control systems can make it possible to compensate for identified deviations.

The aim of this study was to identify and compensate phase deviations of individual elements of multi-element focused ultrasonic systems using the acoustic holography method and assessing the influence of these phase distortions on the shape of the focal lobe. Experimental verification was carried out in water using a 256-element 1.2 MHz focused transducer.

MATERIALS AND METHODS

256-element Focused Fully Populated Array

The 256-element focused piezocomposite array (Imasonic, France) with a diameter of 200 mm, a focal length of 150 mm, and a central frequency of 1.2 MHz was used in the study. The array was designed in the Laboratory for Industrial and Medical Ultrasound of Moscow State University, and its parameters and acoustic characterization were previously reported in [17]. A key feature of this source is the irregular nature of the arrangement of elements having the shape of equal area polygons adjacent to each other with a possible minimum kerf [18, 19]. Such arrays, termed as absolutely dense or fully populated (FPA), have a reduced level of side lobes compared to arrays with periodic arrangement of elements. In addition, FPAs make it possible to achieve higher levels of acoustic pressure at the focus at the same intensity on the surface of the elements due to the beneficial use of almost the entire surface area of the transducer.

A sketch of the element arrangement and a photograph of the source are presented in Figs. 1a and 1b respectively. The nominal kerf between elements is 0.5 mm. The central opening of 40 mm diameter is intended to accommodate a diagnostic ultrasound probe for ultrasound monitoring and visualizing processes in the focal area of the FPA in biological tissues and their phantoms in the thermal ablation [1, 2] and histotripsy studies [3–6].

Scanning the field with a hydrophone (details and parameters of the measuring system are given below) in the focal region during in-phase excitation mode revealed that the shape of the focal region of the beam is asymmetric and different from the theoretically predicted one for a given transducer with uniform surface vibration (Fig. 1c). However, the reasons for such field

distortions were not evident and motivated the proposed study.

Acoustic Holography and Phase Compensation

Acoustic holography is a powerful metrological tool [11] that has been widely used to characterize ultrasonic sources and their fields [10–16]. Below we only present the main aspects of its application to the problem considered here.

A focused ultrasonic transducer operating in continuous mode at angular frequency ω creates an acoustic pressure field in front of it, which can be expressed as follows:

$$p(\mathbf{r},t) = A(\mathbf{r})\cos[\omega t - \varphi(\mathbf{r})] = \mathrm{Re}\left[P(\mathbf{r})e^{-i\omega t}\right]. \quad (1)$$

Here A and φ are the magnitude and phase of the pressure wave, and $P(\mathbf{r},\omega) = Ae^{i\varphi}$ is the complex amplitude.

An acoustic hologram is a two-dimensional distribution of complex amplitude (i.e., the magnitude and phase of the wave) measured along a certain surface $\sum_H$ intersected by an ultrasonic beam. Such a hologram makes it possible to solve the inverse problem of finding the pressure distribution on the surface of the source. One convenient solution is to use the Rayleigh integral [11]:

$$P(\mathbf{r}_S,\omega) = \frac{1}{2\pi}\int_{\sum_H} P(\mathbf{r}_H,\omega)\frac{\partial}{\partial n_H}\left(\frac{e^{-ik|\mathbf{r}_H-\mathbf{r}_S|}}{|\mathbf{r}_H-\mathbf{r}_S|}\right)d\sigma. \quad (2)$$

Here, the position vectors $\mathbf{r}_S$ and $\mathbf{r}_H$ lie on the surfaces of the source $\sum_S$ and the hologram $\sum_H$, respectively, and $\partial/\partial n_H$ is the derivative along the normal to the hologram surface $\sum_H$ facing the transducer. One can also calculate the complex amplitude of the normal component of the vibrational velocity V_n on the surface of the source as

$$V_n(\mathbf{r}_S,\omega) = -\frac{i}{k\rho_0 c_0}\frac{\partial P(\mathbf{r}_S,\omega)}{\partial n_S}. \quad (3)$$

Here ρ_0 is the density and c_0 is the speed of sound in the medium, $k = \omega/c_0$ is the wavenumber, $\partial/\partial n_S$ is the derivative along the outer normal to the surface of the source $\sum_S$. The explicit form of expressions for forward- and backpropagation, taking into account the normal derivatives for the complex amplitudes of acoustic pressure and vibrational velocity in the case of a flat hologram surface and a spherically concave transducer, is given in Appendix A of [11]. While it is the normal vibrational velocity that determines the structure of oscillations of the source surface, in case of an electronic beam (or ray) steering and determining the contribution of the signal of each surface element to the resulting acoustic field in the medium, one can only operate with acoustic pressure values.

In order to determine the phase on the surface of the elements in case of multi-element transducers, surface points $\sum_m \in \sum_S$ corresponding to each single element with number m are selected from the general distribution $P(\mathbf{r}_S,\omega)$. It should be noted that a piezoelectric source can be considered as a linear transducer, therefore the pressure field emitted by a multi-element array, in the linear acoustics regime, can be considered as the sum of the pressure fields emitted by the individual elements:

$$P = \sum_m P_m . \quad (4)$$

The contribution of the m-th element to the acoustic field is the result of an electroacoustic transformation arising from the driving voltage U_m of the corresponding channel. The relationship between P_m and U_m is influenced by the transfer function of the electronic circuit of the generator itself, T_{GENm}, transfer function of the matching network, T_{MNETm}, and transfer function of the piezoelectric transducer, T_{TXm}: $P_m = T_{TXm}T_{MNETm}T_{GENm}U_m$. Possible distortions caused by these factors can be determined by comparing the specified amplitudes and phases on the elements with the actual values obtained from the acoustic hologram by averaging the complex amplitudes over the element surface $\sum_m$. As was analyzed in [16], in the presence of magnitude and phase deviations, the latter provides the main contribution to the distortion of the field structure of multi-element focused sources. The effective phase of the acoustic signal of a given element can be calculated as follows:

$$\Phi_m = \arg\left[\frac{1}{\sum_m}\int_{\sum_m} P(\mathbf{r}_S,\omega)\,d\sigma\right], \quad (5)$$

where "arg" denotes the complex number argument. Note that instead of the pressure in Eq. (5), the phase Φ_m can be calculated for the normal velocity defined by Eq. (3), although if the element diameter is much larger than the wavelength, the corresponding difference is small. The value of Φ_m is determined by the combined contribution of all distorting factors $\Phi_m = \arg(T_{TXm}T_{MNETm}T_{GENm})$, which cannot be explicitly separated using only acoustic holography. However, compensation for the resulting phase deviations without separating different contributions is more essential for practical implementations. To do this, it is sufficient to introduce phase correction factors in the form of inverted phase values $\Phi_{m\_COR} = -\Phi_m$ into each channel of the driving system:

$$U_{m\_COR} = U_m e^{i\Phi_{m\_COR}} = U_m e^{-i\Phi_m}. \quad (6)$$

Experimental Data Acquisition and Processing

To characterize the 256-element fully populated transducer array considered here (Fig. 1) by acoustic holography, an experimental setup based on an automated CNC scanning system (UMS3, Precision Acoustics, UK) with a linear displacement range of $0.4 \times 0.4 \times 0.8$ m was used, allowing for moving the hydrophone in 1 micron increments with a guaranteed positioning accuracy of up to 5 microns. The system was placed above a water tank in which the transducer and the hydrophone were located. The reservoir was filled with purified degassed water (WTS water treatment system, Precision Acoustics, UK) to a dissolved oxygen concentration levels of 3–4 mg/L. Prior to the measurements, water was heated to room temperature about 23°C and thermostated during the measurements with an accuracy of 0.2°C. The FPA transducer, fixed in water, was driven by a 256-channel V1 Verasonics Data Acquisition system (VDAS, Verasonics Inc., USA).

To simultaneously measure multiple CW holograms at different frequencies, the transient (pulsed) acoustic holography method was used [12, 20, 21]. Short pulses consisting of 3 periods of the 1.2 MHz central frequency were applied to each channel. The resulting acoustic field was recorded using an HGL-0200 hydrophone with AH-2010-100 preamplifier (Onda, UK) and a TDS5054B oscilloscope (Tektronix, USA). In order to improve signal to noise ratio (SNR), waveform averaging over 32 samples was performed for each spatial measurement point in a window of 100 μs with a sampling frequency of 50 MHz, after which the averaged waveform was transferred via the GPIB to a computer for further processing. The oscilloscope trigger with a fixed delay (depending on the distance between the transducer and the hydrophone) was synchronized with firing of the first array element by an external trigger of the VDAS.

Field scanning in the focal area was carried out at the minimum VDAS input level (up to 3.6 V) to minimize the risk of damage to the hydrophone. Measurements along the hologram plane, which was located 40 mm prefocally perpendicular to the transducer acoustic axis, were carried out at a VDAS input levels of 3.6 V and below. The acoustic hologram was recorded in the nodes of a square grid of 251×251 size with a step of 0.5 mm, which corresponded to a region of 125×125 mm. First, acoustic pressure field measurements were performed for the in-phase VDAS operation mode in the focal region and along the hologram, which made it possible to capture the distortion of the focal region and determine the phase shifts Φ_m, Eq. (5). Figure 2a and 2b show the distributions of the acoustic pressure magnitude and phase, respectively, on the surface of the hologram at a frequency of 1.2 MHz. Figures 2c and 2d contain the amplitude and phase distributions for the same frequency on a spherical surface with a radius of curvature of 150 mm. After introducing phase compensation, Eq. (6), into the channels of driving system, measurements for the same positions were repeated to estimate the quality of the correction.

RESULTS AND DISCUSSION

When recording pulsed signals, the transient hologram was processed to obtain a set of the monochromatic holograms [12, 20, 21]. The hologram that corresponds to the central frequency of the transducer (1.2 MHz) was chosen for subsequent analysis of phase compensation. The dimensions of the transducer array and the hologram region were significantly larger than the wavelength, therefore small angular deviation between the acoustic axis and one of the mechanical axes of the scanning system could lead to additional phase discrepancy after holographic processing. Such misalignment-induced phase shifts can be determined and compensated by rotating the hologram plane when calculating the integral in Eq. (3) based on previously developed algorithms [22, 23]. Figure 3 shows the phase distribution fields on a spherical surface with a radius of curvature of 150 mm, located at a distance of 110 mm from the hologram plane. Figure 3a corresponds to the calculation of the original hologram and duplicates Fig. 2b for convenience of comparison with other distributions. Figure 3b shows the results of backpropagation with accounting for the misalignment of axes using the hologram rotation. Fig. 3c represents the phase distribution along the surface of the array after introducing the channel-by-channel phase compensation Φ_m, shown in Fig. 3d for each channel. The amplitude distributions after rotating the hologram and introducing phase compensation were practically the same as the initial one presented in Fig. 2c.

The results shown in Fig. 3c demonstrate that introducing the channel-by-channel phase compensation into the VDAS driving signals leads to significantly more uniform phase distribution along the transducer surface. Meanwhile, the resulting distribution still remains uneven. This inhomogeneity can be reduced by iterative application of the proposed procedure, but due to time-consuming hologram measurements for such big source (more than 15 h), this method is not always optimal. The quality of the phase compensation can be assessed by various metrics, among which the parameters of focal region are widely used for focused sources: focusing gain, longitudinal and transverse dimensions, shape (at given levels). As already noted, the premise of this work is the detected deviation of the shape of the focal region of the beam in axial sections from the nominal one. It is therefore reasonable to evaluate the influence of the introduced phase compensation on the shape of the focus in the same sections. Figure 4 represents holographic reconstruction of the focal region of the beam for in-phase VDAS generation (4a, 4b) and after phase correction

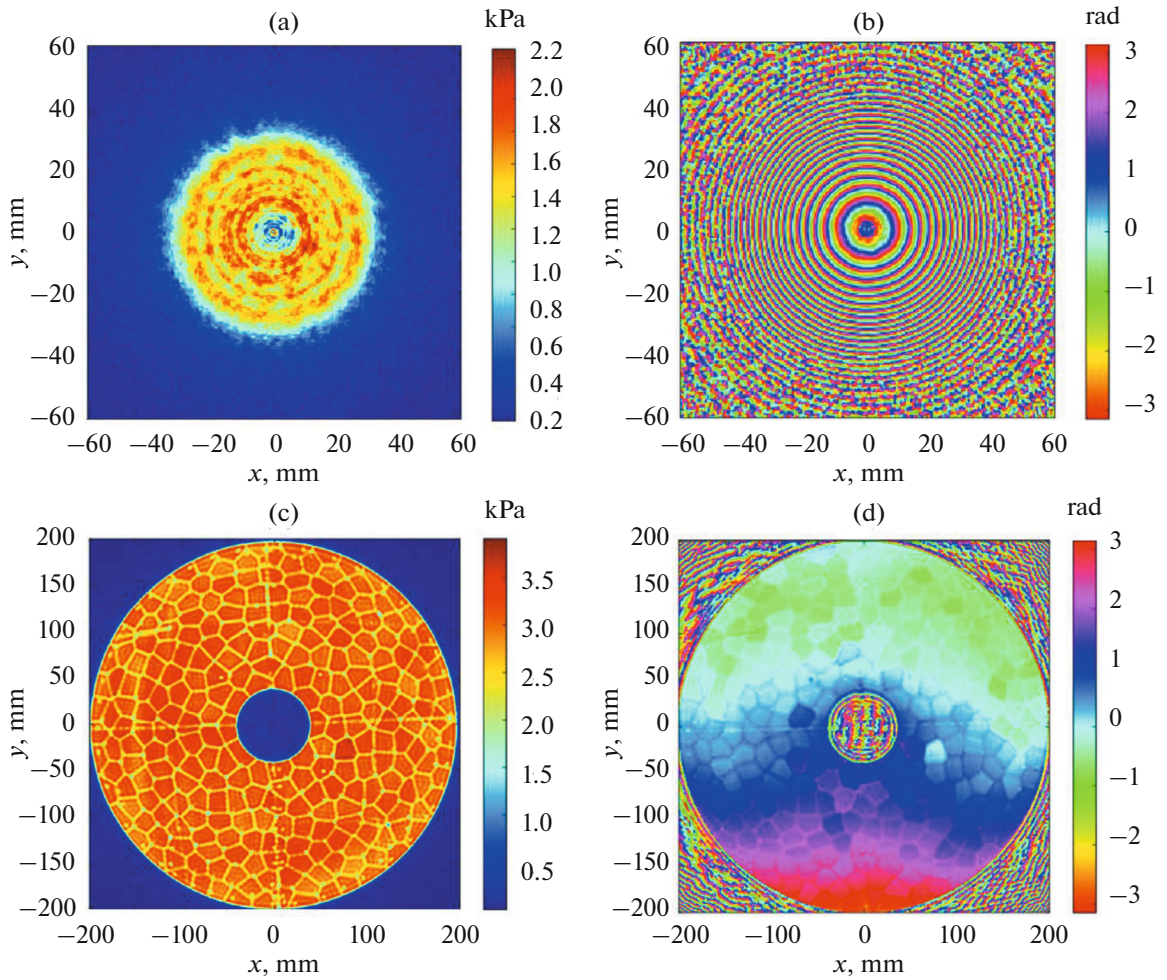

Fig. 2. Monochromatic hologram for 1.2 MHz frequency at 3.6 V VDAS input. (a) Distribution of the acoustic pressure magnitude along a 40 mm prefocal measurement plane. (b) Distribution of the acoustic pressure phase in the same plane. (c, d) Holographic reconstruction of the amplitude (c) and phase (d) distributions of normal component of vibrational velocity along the spherical transducer surface.

(4c, 4d). 3D plots show acoustic pressure isosurfaces at −6 (red) and −12 dB (yellow) levels referencing absolute focal maximum for each case. 2D distributions correspond to vertical (*YZ*) and horizontal (*XZ*) sections. Asymmetry of the initial distribution (4a, 4b) can be clearly seen and corresponds well to first hydrophone scans (see Fig. 1c). After phase correction procedure, the shape becomes much more symmetrical. Axial (z and x) distributions of acoustic pressure amplitude for initial in-phase signals (gray line) and phase-corrected signals (black line) reconstructed from holograms (Figs. 4e, 4f) show 14% peak pressure growth after phase deviations compensation (28 vs. 24.5 kPa) for the same amplitude VDAS input level of 3.6 V. Holographic reconstruction corresponds well to independent hydrophone measurements (dots in Figs. 4e, 4f). The obtained results show almost complete shape recovery of the focal region of the beam and significant growth of the peak pressure value after implementing the phase shifts.

By analyzing phase deviations Φ_m extracted from the measured hologram (Fig. 3d), we may suggest their origin. While the phase distribution (Fig. 3b) looks almost symmetrical relative to the vertical axis, a horizontal "cut" line dividing the surface into two halves is visible on the surface of the source (refer also to magnitude in Fig. 2c). It is reasonable to assume therefore that in the manufacturing process of the piezocomposite bowl of the transducer, mechanical stresses leading to deviation of the surface shape from spherical to ellipsoidal were introduced. This can be assessed by paying attention to the LMS trend line (solid in Fig. 3d), which occupies a phase interval of about 50 degrees and corresponds to an estimated linear deviation value of 150 μm. Dashed line in Fig. 3d shows constant phase as a reference for an ideally spherical surface. For a transducer with a surface cur-

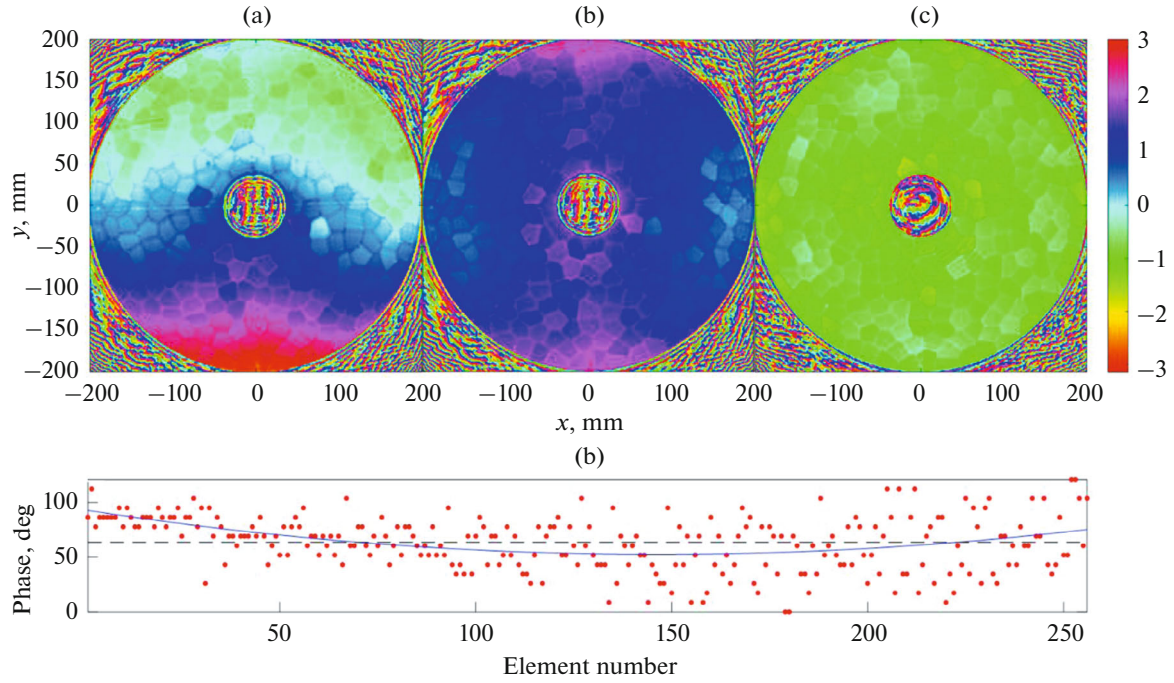

Fig. 3. Phase distributions for 1.2 MHz frequency on a spherical surface with a radius of curvature of 150 mm. (a) Direct reconstruction from the hologram shown in Figs. 2a, 2b for in-phase VDAS driving mode. (b) Reconstruction from the same hologram after accounting for misalignment of transducer acoustical axis and z-axis of the scanning system. (c) Phase distribution along the surface of the source after introducing the channel-by-channel phase compensation. (d) Values of phase shift Φ_m for each element $m \in [1, 256]$ are shown by red dots. Blue solid line represents LMS trend to find surface asphericity. Dashed line corresponds to an ideal sphere.

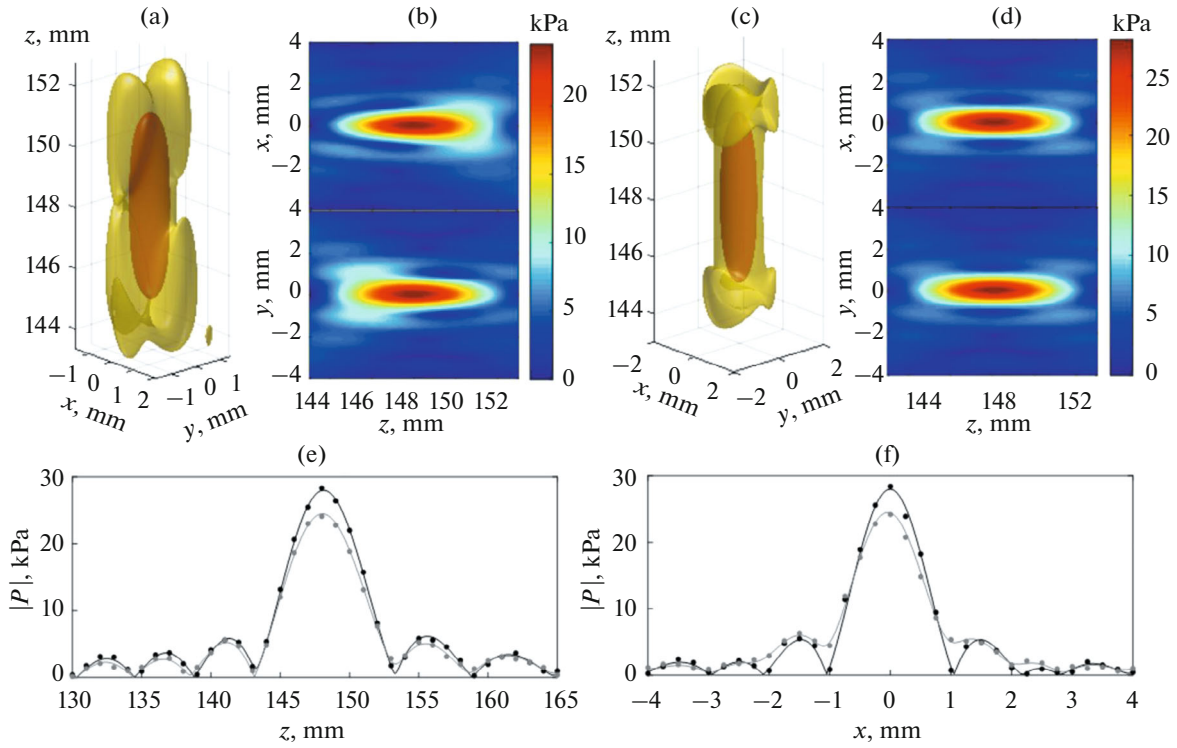

Fig. 4. Shape of the focal region of the beam for (a, b) in-phase VDAS generation and (c, d) after phase correction reconstructed from the holograms. (a, c) Acoustic pressure isosurfaces at −6 (red) and −12 dB (yellow) levels referencing absolute focal maximum for each case. (b, d) Horizontal (top) and vertical (bottom) sections of the focal region. (e, f) Axial (z and x, respectively) distributions of the acoustic pressure amplitude for initial in-phase signals (gray line) and phase-corrected signals (black line) reconstructed from holograms. Dots represent results of the independent hydrophone measurements.

vature radius of 150 mm and a diameter of 200 mm, such deviation is a very insignificant, which, nevertheless, may distort a focal region of the beam. Irregular deviations of Φ_m from the trend line (Fig. 3d) may correspond to discrepancy between channel transfer functions of VDAS $T_{\mathrm{GEN}m}$ and matching network $T_{\mathrm{MNET}m}$, which are described by the contribution of the P_m term in Eq. (4).

CONCLUSIONS

Multi-element ultrasonic systems may have unaccounted sources of uncertainty in the operating phases at their elements, resulting in noticeable distortions in the acoustic field pattern compared to the theoretically predicted one. The method presented here determines and compensates for element-by-element phase deviations using acoustic holography, enabling the generation of fields with a predictable spatial structure. This capability is especially important in medical and industrial applications of high-intensity focused ultrasound.

FUNDING

The study was supported by the Russian Science Foundation (project no. 22-22-00751).

CONFLICT OF INTEREST

The authors of this work declare that they have no conflicts of interest.

REFERENCES

1. G. T. Haar, Ultrasound. Med. Biol. **21** (9), 1089 (1995). https://doi.org/10.1016/0301-5629(95)02010-1
2. G. T. Haar and C. Coussios, Int. J. Hyperthermia. **23** (2), 89 (2007). https://doi.org/10.1080/02656730601186138
3. M. S. Canney, V. A. Khokhlova, O. V. Bessonova, M. R. Bailey, and L. A. Crum, Ultrasound Med. Biol. **36** (2), 250 (2010). https://doi.org/10.1016/j.ultrasmedbio.2009.09.010
4. T. D. Khokhlova, M. S. Canney, V. A. Khokhlova, O. A. Sapozhnikov, L. A. Crum, and M. R. Bailey, J. Acoust. Soc. Am. **130** (5), 3498 (2011). https://doi.org/10.1121/1.3626152
5. Z. Xu, T. L. Hall, E. Vlaisavljevich, and F. T. Lee, Jr., Int. J. Hyperthermia **38** (1), 561 (2021). https://doi.org/10.1080/02656736.2021.1905189
6. V. A. Khokhlova, P. B Rosnitskiy, S. A. Tsysar, S. V. Buravkov, E. M. Ponomarchuk, O. A. Sapozhnikov, M. M. Karzova, T. D. Khokhlova, A. D. Maxwell, Y.-N. Wang, A. V. Kadrev, A. L. Chernyaev, V. P. Chernikov, D. A. Okhobotov, A. A. Kamalov, and G. R. Schade, Ultrasound Med. Biol. **49** (1), 62 (2023). https://doi.org/10.1016/j.ultrasmedbio.2022.07.014
7. V. G. Andreev, V. N. Dmitriev, Y. A. Pishchalnikov, O. V. Rudenko, O. A. Sapozhnikov, and A. P. Sarvazyan, Acoust. Phys. **43** (2), 123 (1997).
8. A. P. Sarvazyan, O. V. Rudenko, and M. Fatemi, IEEE Trans. Ultrason. Ferroelectr. Freq. Control. **68** (11), 3261 (2021). https://doi.org/10.1109/TUFFC.2021.3112505
9. J. R. Doherty, G. E. Trahey, K. R. Nightingale, and M. L. Palmeri, IEEE Trans. Ultrason. Ferroelectr. Freq. Control. **60** (4), 685 (2013). https://doi.org/10.1109/tuffc.2013.2617
10. O. A. Sapozhnikov, Y. A. Pishchalnikov, and A. V. Morozov, Acoust. Phys. **49** (3), 354 (2003)
11. O. A. Sapozhnikov, S. A. Tsysar; V. A. Khokhlova, and W. Kreider, J. Acoust. Soc. Am. **138** (3), 1515 (2015). https://doi.org/10.1121/1.4928396
12. S. A. Tsysar, D. A. Nikolaev, and O. A. Sapozhnikov, Acoust. Phys. **67** (3), 320 (2021). https://doi.org/10.1134/S1063771021030131
13. W. Kreider, P. V. Yuldashev, O. A. Sapozhnikov, N. Farr, A. Partanen, M. R. Bailey, and V. A. Khokhlova, IEEE Trans. Ultrason. Ferroelectr. Freq. Control. **60** (8), 1683 (2013). https://doi.org/10.1109/TUFFC.2013.2750
14. E. M. Ponomarchuk, P. V. Yuldashev, D. A. Nikolaev, S. A. Tsysar, A. A. Mironova, and V. A. Khokhlova, Acoust. Phys. **69** (4), 459 (2023). https://doi.org/10.1134/S1063771023600560
15. E. Martin, M. Roberts, and B. Treeby, JASA Express Lett. **1**, 012001 (2021). https://doi.org/10.1121/10.0003210
16. M. A. Ghanem, A. D. Maxwell, W. Kreider, B. W. Cunitz, V. A. Khokhlova, O. A. Sapozhnikov, and M. R. Bailey, IEEE Trans. Ultrason. Ferroelectr. Freq. Control. **65** (9), 1618 (2018). https://doi.org/10.1109/TUFFC.2018.2851188
17. O. A. Sapozhnikov, P. B. Rosnitskiy, S. A. Asfandiyarov, D. A. Nikolaev, S. A. Tsysar, and V. A. Khokhlova, J. Acoust. Soc. Am. **150** (4), A84 (2021). https://doi.org/10.1121/10.0007705

18. P. B. Rosnitskiy, B. A. Vysokanov, L. R. Gavrilov, O. A. Sapozhnikov, and V. A. Khokhlova, IEEE Trans. Ultrason. Ferroelectr. Freq. Control. **65** (4), 630 (2018). https://doi.org/10.1109/TUFFC.2018.2800160

19. P. B. Rosnitskiy, O. A. Sapozhnikov, L. R. Gavrilov, and V. A. Khokhlova, Acoust. Phys. **66** (4), 352 (2020). https://doi.org/10.1134/S1063771020040090

20. O. A. Sapozhnikov, A. E. Ponomarev, and M. A. Smagin, Acoust. Phys., **52** (3), 324 (2006).

21. D. A. Nikolaev, S. A. Tsysar, V. A. Khokhlova, W. Kreider, and O. A. Sapozhnikov, J. Acoust. Soc. Am. **149** (1), 386 (2021). https://doi.org/10.1121/10.0003212

22. S. A. Tsysar, O. A. Sapozhnikov, S. N. Gurbatov, I. Y. Demin, and N. V. Pronchatov-Rubtsov, Bull. Nizhny Novgorod Univ. **1** (3), 230 (2013).

23. A. Z. Kaloev, D. A. Nikolaev, V. A. Khokhlova, S. A. Tsysar, and O. A. Sapozhnikov, Acoust. Phys. **68** (1), 71 (2022). https://doi.org/10.1134/S1063771022010043